Contrib Mineral Petrol (2005) 148: 746–760
DOI 10.1007/s00410-004-0637-4

ORIGINAL PAPER

J. Hermann · H. S. C. O'Neill · A. J. Berry

Titanium solubility in olivine in the system TiO_2–MgO–SiO_2: no evidence for an ultra-deep origin of Ti-bearing olivine

Received: 1 June 2004 / Accepted: 25 October 2004 / Published online: 1 December 2004

Abstract The finding of ilmenite rods in olivine from orogenic peridotites has sparked a discussion about the processes of incorporation and exsolution of titanium in olivine. We have experimentally investigated the solubility of Ti in olivine as a function of composition, temperature and pressure in the synthetic TiO_2–MgO–SiO_2 system. Experiments at atmospheric pressure in the temperature range 1,200–1,500°C showed that the highest concentration of TiO_2 is obtained when olivine coexists with spinel (Mg_2TiO_4). The amount of TiO_2 in olivine in the assemblages olivine + spinel + periclase and olivine + spinel + ilmenite at 1,500°C was 1.25 wt.%. Changes in the coexisting phases and decreasing temperature result in a significant reduction of the Ti solubility. Olivine coexisting with pseudobrookite ($MgTi_2O_5$) and a Ti–Si-rich melt at 1,500°C displays a fourfold lower TiO_2 content than when buffered with spinel. A similar decrease in solubility is obtained by a decrease in temperature to 1,200°C. There is a negative correlation between Ti and Si and no correlation between Ti and Mg in Ti-bearing olivine. Together with the established phase relations this suggests that there is a direct substitution of Ti for Si at these temperatures, such that the substituting component has the stoichiometry Mg_2TiO_4. The unit cell volume of olivine increases systematically with increasing TiO_2 content demonstrating that the measured TiO_2 contents in olivine are not caused by micro-inclusions but by incorporation of Ti in the olivine structure. Least squares fitting of 20 olivine unit cell volumes against the Ti content yield the relation: V (Å^3) = 290.12(1) + 23.67(85) N_{Ti}. The partial molar volume of end-member Mg_2TiO_4 olivine ($N_{Ti} = 1$) is thus 47.24 ± 0.13 cm^3. The change of the Ti solubilty in olivine coexistent with rutile and orthopyroxene with pressure was investigated by piston cylinder experiments at 1,400°C from 15 to 55 kbar. There is no increase in TiO_2 contents with pressure and in all the experiments olivine contains ~0.2 wt.% TiO_2. Moreover, a thermodynamic analysis indicates that Ti contents of olivine coexisting with rutile and orthopyroxene should decrease rather than increase with increasing pressure. These data indicate that the ilmenite exsolution observed in some natural olivine does not signify an ultra-deep origin of peridotite massifs.

Editorial Responsibility: J. Hoefs

J. Hermann (✉) · H. S. C. O'Neill · A. J. Berry
Research School of Earth Sciences,
Australian National University,
Canberra, ACT, 0200, Australia
E-mail: joerg.hermann@anu.edu.au

Introduction

The finding of oriented ilmenite inclusions (rods) in olivine from the Alpe Arami peridotite (central Alps, Switzerland) has led to the suggestion that these rocks originated from the mantle transition zone and thus preserve evidence for the greatest depth of origin of any rock outcropping on the Earth's surface (Dobrzhinetskaya et al. 1996; Green et al. 1997). This interpretation has not gone unchallenged, and has sparked a wide-ranging discussion on the origin and significance of such Ti-phase exsolution in olivine. Initially it was argued that high Ti solubility is only possible in the wadsleyite stability field and that the exsolution is related to decompression (Dobrzhinetskaya et al. 1996; Green et al. 1997). Later research questioned this hypothesis because olivine with ilmenite rods was also discovered at other localities, where the maximum pressure did not exceed 40–50 kbar (Hacker et al. 1997; Trommsdorff et al. 2000; Risold 2001). An alternative explanation was proposed by Risold et al. (2001) who observed that occasionally the rods are aligned in palisades within olivine. They suggested that the ilmenite rods form from dehydration of titanian-clinohumite defect layers at P~30 kbar and T~800°C.

Irrespective of the interpretation, the presence of ilmenite exsolution in olivine demonstrates that the Ti

solubility can be significant under certain conditions. On the basis of image analysis it was suggested that up to 0.7 wt.% TiO_2 was incorporated in Alpe Arami olivine prior to exsolution (Dobrzhinetskaya et al. 1996; Green et al. 1997) although this high value has not been confirmed by other methods. Microprobe scan analyses indicate that the olivine grains with the densest population of ilmenite rods contain ~330 ppm TiO_2 (Hacker et al. 1997), while laser-ablation ICP-MS yields similar values of up to 350 ppm (Reusser et al. 1998). These amounts are within the upper limit of TiO_2 contents found in olivine from mantle xenoliths (Hervig et al. 1986).

Experimental studies on Ti solubility in olivine are also controversial. Ulmer et al. (1998) found 0.135 wt.% TiO_2 in olivine at 1,400°C and 0.105 wt.% TiO_2 at 1,200°C in the paragenesis olivine + ilmenite + water in a natural system. They reported no pressure dependence on the TiO_2 content of olivine in the range from 10 to 90 kbar. In contrast, other studies suggested that there is a strong increase in Ti-solubility with pressure (Dobrzhinetskaya et al. 1999; Tinker and Lesher 2001). Dobrzhinetskaya et al. (1999) report maximum values above 1 wt.% TiO_2 in olivine at 120 kbar and 1,177–1,327°C for a lherzolite doped with ilmenite. On the other hand, at 140 kbar Gudfinsson and Wood (1998) measured only 0.07 and 0.11 wt.% TiO_2 in olivine coexisting with ilmenite at 1,400 and 1,600°C, respectively. O'Neill (1998) demonstrated that Fe–Mn olivine can incorporate more than 1 wt.% of TiO_2 at 1,100°C in 1 atm experiments, but only about half this amount at 25 kb and the same temperature. He also pointed out that the decrease in the solubility of Ti in olivine with increasing pressure is expected from thermodynamic considerations, if TiO_2 occurs as a component with M_2TiO_4 stoichiometry. Although this stoichiometry was indicated by his experiments, it is not compatible with the common observation of ilmenite ($MTiO_3$) exsolution in natural olivine.

In this paper, we address these controversies through an experimental study on the solubility of Ti in olivine as a function of bulk composition and temperature in the $MgO–SiO_2–TiO_2$ system at atmospheric pressures. Additionally, piston cylinder experiments were undertaken to determine the Ti solubility at higher pressure. These results were then combined with measurements of the molar volumes of Ti-olivine to evaluate the relative effects of temperature, pressure and bulk composition on the solubility of Ti in olivine, and hence the significance of both the amounts observed in natural olivine and the exsolution of ilmenite rods.

Experimental strategy

A series of experiments at atmospheric pressure were carried out on different compositions from 1,200 to 1,500°C, to evaluate the effect of temperature and composition on the solubility of Ti in olivine. We have chosen the simple system $MgO–SiO_2–TiO_2$ to avoid problems with the variable oxidation state of Fe and to minimize problems with Ti Kα fluorescence caused by Fe Kα excitation (Feenstra and Engi 1998).

Previous experiments in the system $MgO–SiO_2–TiO_2$ (MacGregor 1969) established the basic phase relations at atmospheric pressure (Fig. 1). Guided by these relations, we produced four starting materials with different amounts of the components forsterite, periclase, qandilite, geikielite, karrooite and enstatite (Tables 1, 2). At

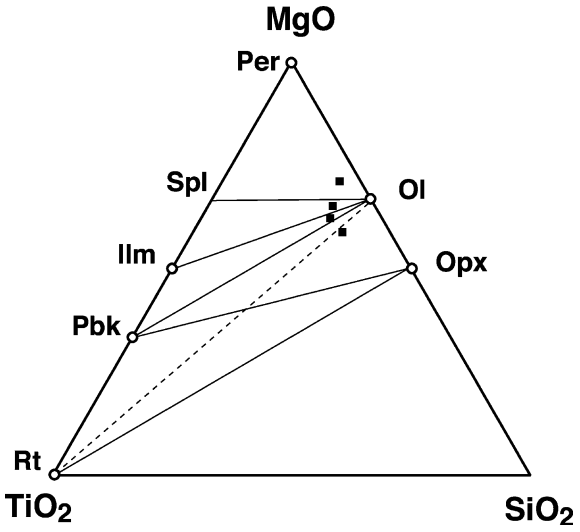

Fig. 1 Simplified phase relations at 1,400°C and 1 atm (after MacGregor 1969). At ~14 kbar the reaction ko + en = fo + rt occurs (*dashed line*). The various starting materials used in the experiments are shown by *filled squares*

Table 1 Abbreviations of phases and components

Phase	Component/endmember
Olivine (Ol)	Forsterite (Mg_2SiO_4) (fo)
Orthopyroxene (Opx)	Enstatite ($Mg_2Si_2O_6$) (en)
Periclase (Per)	Periclase (MgO) (per)
Ilmenite (Ilm)	Geikielite ($MgTiO_3$) (gk)
Spinel (Spl)	Qandilite (Mg_2TiO_4) (qd)
Pseudobrookite (Pbk)	Karrooite ($MgTi_2O_5$) (ko)
Rutile (Rt)	Rutile (TiO_2) (rt)
Melt (M)	

Table 2 Starting compositions, expressed as % of endmember components, for experiments at atmospheric pressure

Composition	I	II	III	IV	V	VI	VII
fo	80	80	80				70
Ti-fo				80	80	80	
per	10			10			
qd	10	10		10	10		
gk		10	10		10	10	
ko			10			10	15
en							15

Abbreviations are given in Table 1. Ti-fo represents forsterite containing ~1 wt.% of TiO_2

atmospheric pressure the paragenesis olivine + rutile is not stable (MacGregor 1969). To verify the attainment of equilibrium we also ran compositional reversals using an olivine synthesised with a high Ti content (~1 wt.% TiO_2) in three starting compositions. Six to seven compositions were run together ensuring exactly the same conditions for a set of experiments.

At high pressures pseudobrookite reacts with orthopyroxene to produce olivine plus rutile (MacGregor 1969)

$$2MgTi_2O_5 + Mg_2Si_2O_6 = 2Mg_2SiO_4 + 4TiO_2. \quad (1)$$

Consequently to determine the pressure dependence of the Ti solubility we synthesised olivine coexistent with orthopyroxene and rutile over a series of pressures at 1,400°C.

Experimental and analytical techniques

The components forsterite, enstatite, qandilite, geikieleit and karrooite used in the starting mixtures were synthesised at 1,000–1,480°C in air for 12 h from fired oxide mixes. To synthesise compositionally homogenous Ti-bearing forsterite, a gel using $Ti(OC_2H_5)_4$ and $Si(OC_2H_5)_4$ was prepared in the stoichiometry $Si_{0.99}Ti_{0.01}O_2$ (Hamilton and Henderson 1968). The dried gel was then mixed with a stoichiometric amount of MgO, pressed into a pellet, and sintered at 1,600°C and 1 atm for 24 h. The starting mixes were obtained from blending the components in the proportions given in Table 2 and homogenising them by grinding in an agate mortar under acetone. The starting composition for the piston cylinder experiments consists of an oxide mix with a composition corresponding to 15% rutile, 25% orthopyroxene and 60% olivine.

For the 1 atm experiments, the starting materials were pressed into pellets using a 4 mm diameter tungsten carbide dye. The samples were placed in baskets made from Pt wire and four to seven baskets were suspended from a Pt ring. This ring was suspended from an alumina tube in the hot spot of a vertical tube furnace. Temperatures were controlled using a type B Pt/Rh thermocouple and are accurate to ±2°C. Run durations were between 4 and 31 days (Table 3). The samples were quenched by dropping onto a metal plate at the base of the furnace. For further details see O'Neill (1998).

For the high-pressure experiments, ~15 mg of the oxide mix was loaded in a Pt capsule, which was sealed by arc welding. The capsule was placed in a MgO tube, inside a teflon foil-NaCl-graphite-pyrex assembly. Synthesis experiments were run in end-loaded 1.27 cm piston-cylinder apparatuses. Pressure was calculated from the direct conversion of load to pressure (low friction assembly) and is accurate to ±0.1 GPa. For the 45 and 55 kbar runs, the samples were left at 800°C and 45 kbar for at least 12 h, which allowed the assembly to compact and remove internal friction. The piston travel in these ultra-high pressure piston cylinder experiments was monitored for the duration of the experiment. The piston travel was very small after the equilibration time of 12 h, indicating that pressure can be calculated from the load applied to the piston. A detailed description of this method and calibration experiments using the fayalite-spinel (Fe_2SiO_4) transition will be presented elsewhere. The temperature was then increased to 1,400°C, the pressure adjusted, and the experiment run for 48 h. Temperature was controlled using type B thermocouples ($Pt_{94}Rh_6/Pt_{70}Rh_{30}$) to ±1°C and is accurate to ±10°C.

The recovered samples were mounted in epoxy and ground down until a representative section was exposed. The phase relations were obtained from detailed studies of backscattered electron (BSE) images. Phase compositions were determined by wavelength dispersive spectrometry (WDS) using a Cameca Camebax electron microprobe with an acceleration voltage of 25 kV and a beam current of 30 nA, and by a Cameca SX-100 operating at 15 kV and a beam current of 20 nA. Samples were also analysed by energy dispersive spectrometry (EDS) using the Cameca Camebax microprobe (15 kV, 6 nA) and with a JEOL 6400 SEM equipped with an EDS detector (15 kV, 1 nA). Analysis of Ti in olivine was difficult because it was often neighboured by a Ti-rich phase leading to analytical artefacts. Because of the generally high Ti contents in experiments at 1,400°C and 1,500°C, we were able to analyse olivine crystals by both WDS and SEM-EDS. The excitation volume using SEM-EDS with a beam current of only 1 nA is much smaller than with WDS, minimising contamination. All analyses were assisted by detailed BSE imaging and only large grains were chosen. Despite these precautions, some olivine crystals showed anomalously high Ti contents. Such analyses were rejected; the reported Ti concentrations are thus obtained from a large population of analyses showing a symmetric Gaussian distribution, with anomalous outliers removed. This approach gives the same results using both WDS and SEM-EDS, within error. Olivine crystals coexisting with melt are up to 300 μm in diameter and thus could be easily analysed by WDS.

Phantom Ti in olivine: an analytical artefact

The piston cylinder experiments were exceptionally difficult to analyse. The TiO_2 content of olivine was generally low, the grain size was small and olivine was in contact with rutile (pure TiO_2). In such a situation, stray electrons or secondary fluorescence can cause artificially high TiO_2 values (see Capabianco and Amelin (1994) for a detailed example of this effect). To test this effect in the present context on the SX-100 electron microprobe we prepared two samples in which a large natural rutile crystal was juxtaposed with either San Carlos olivine or synthetic periclase. The San Carlos olivine has almost negligible Ti (< 10 ppm), while any Ti in the synthetic periclase is below the detection limit. The sample pairs

were sectioned and polished, pressed together, mounted in epoxy and sectioned normal to the interface (as one might do for a diffusion couple). The couples were then analysed for Ti using the electron microprobe by profiling over the contact zone (Fig. 2). Unfortunately there was a 30–50 μm gap filled with epoxy between the faces of the crystals in both couples. The apparent TiO_2 contents obtained from the epoxy decreased from about 0.45 to 0.2 wt.% in this zone. In the San Carlos olivine, the amount of phantom TiO_2 then jumped to 0.35 wt.% at its interface with epoxy; this is presumably due to secondary fluorescence from Fe in the olivine, since there is essentially no jump in the phantom TiO_2 for periclase. Nevertheless, the amount of phantom TiO_2 in the periclase is 0.2 wt.% at its interface; this is coincidentally similar to what is believed to be the saturation level of forsterite synthesised in the high-pressure experiments. The concentration of TiO_2 in both olivine and periclase then decreases exponentially with distance and after ~100 μm reaches the detection limits. Similar experiments documenting this effect for Fe, Cr and Ni in glass adjacent to metal have been described by Capobianco and Amelin (1994), and for Ca in olivine by Dalton and Lane (1996). The important observation, as emphasised by Capobianco and Amelin (1994), is that phantom amounts of an element (at the $\sim 10^3$ ppm level) can be detected when the target crystal is adjacent to a phase containing high concentrations of that element; this happens even when the target crystal does not contain any elements with sufficiently high X-ray emission energies to excite fluorescence in the adjacent phase—the example here being MgO. This may be due either to stray electrons or flourescence from background Bremstrahlung radiation.

To overcome this problem, our samples were ground lightly in a mortar to separate the crystals and the

Table 3 Ti contents of olivine are given in wt.% TiO_2 and as cations per formula unit (pfu). The unit cell volume was determined for selected samples. Most of the samples were prepared under subsolidus conditions. In silica-rich compositions a Si-Ti-rich melt formed at high temperatures; traces of melt are indicated by ±M. Abbreviations are given in Table 1

Mix	Run products	TiO_2 wt.%	Ti (pfu)	Unit cell volume (Å^3)
1,500°C run#: B 29/6/00 4 days				
I	Per + Spl + Ol	1.24 (5)	0.022 (1)	290.637 (7)
II	Spl + Ilm + Ol	1.26 (7)	0.022 (1)	290.651 (7)
III	Pbk + Ol	0.87 (4)	0.015 (1)	290.473 (6)
IV	Per + Spl + Ol	1.18 (8)	0.021 (1)	290.649 (7)
V	Spl + Ilm + Ol	1.29 (5)	0.023 (1)	290.693 (7)
VI	Pbk + Ol ± M	0.68 (11)	0.012 (2)	
VII	Pbk + Ol + M	0.31 (5)	0.0054 (8)	290.232 (8)
1,400°C-1 run#: B16/6/00 5 days				
I	Per + Spl + Ol	0.92 (9)	0.016 (2)	290.493 (8)
II	Spl + Ilm + Ol	0.97 (9)	0.017 (2)	290.470 (6)
III	Ilm + Pbk + Ol	0.49 (9)	0.0087 (15)	290.354 (7)
IV	Per + Spl + Ol	1.00 (10)	0.018 (2)	290.433 (8)
V	Spl + Ilm + Ol	0.95 (10)	0.017 (2)	290.464 (7)
VI	Pbk + Ol	0.34 (7)	0.0060 (11)	290.285 (7)
1,400°C-2 run#: D 24/10/00 31 days				
I	Per + Spl + Ol	0.94 (8)	0.016 (1)	
II	Spl + Ilm + Ol	0.99 (7)	0.017 (1)	
III	Ilm + Pbk + Ol	0.43 (7)	0.0080 (11)	290.359 (8)
IV	Per + Spl + Ol	0.94 (6)	0.017 (1)	290.539 (9)
V	failed			
VI	Pbk + Ol	0.21 (2)	0.0037 (4)	290.266 (8)
VII	Pbk + Ol + M	0.19 (2)	0.0033 (3)	290.216 (10)
1,200°C-1 run#: B 17/7/00 31 days				
I	Per + Spl + Ol	0.33 (8)	0.0057 (15)	290.148 (11)
II	Spl + Kor + Ol	0.27 (5)	0.0049 (9)	290.233 (13)
III	Ilm + Pbk + Ol	0.19 (5)	0.0034 (10)	290.175 (10)
IV	Per + Spl + Ol	0.26 (6)	0.0047 (11)	290.279 (11)
V	Spl + Ilm + Ol	-	-	290.228 (12)
VI	Pbk + Ol	-	-	290.186 (11)
VII	Pbk + Opx + Ol	0.088 (43)	0.0016 (8)	290.159 (12)
1,300°C run#: D 19/1/01 18 days; + 10% diopside-anorthite eutectic flux				
II	Pbk + Ol + M	0.22 (1)	0.0039 (2)	
1,300°C run#: D 28/3/01 7 days; + 10% Na-K flux				
I	Per + Spl + Ol ± M	0.75 (14)	0.013 (2)	
III	Pbk + Ol ± M	0.37 (10)	0.0065 (18)	
VII	Pbk + Ol + M	0.23 (5)	0.0040 (9)	
1,200°C run#: D 23/4/01 7 days; + 10% Na-B flux				
I	Per + Spl + Ol ± M	1.20 (14)	0.021 (3)	
II	Spl + Ilm + Ol ± M	0.76 (10)	0.013 (2)	
III	Ilm + Pbk + Ol ± M	0.37 (12)	0.0064 (21)	
VII	Pbk + Ol + M	0.25 (3)	0.0044 (4)	

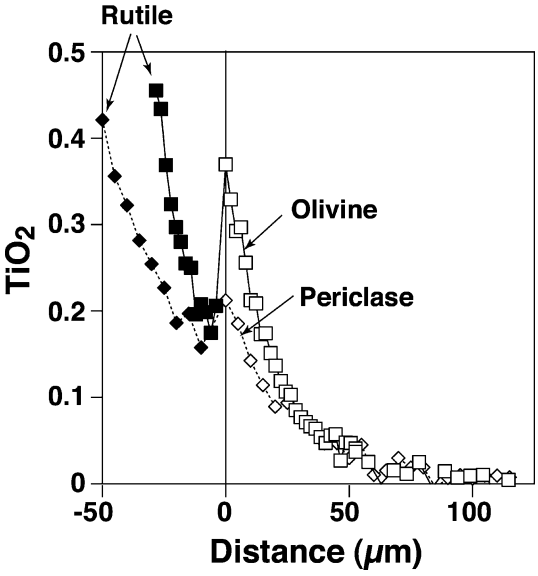

Fig. 2 Apparent TiO_2 concentration profiles from rutile through epoxy to either San Carlos olivine or periclase. The points measured in the epoxy are given by *solid symbols* and analyses in olivine/periclase as *open symbols*. The first point in epoxy corresponds to the rutile/epoxy interface and the epoxy/sample interface is the 0 reference for distance. The measured increase in TiO_2 concentration towards rutile in both, olivine and periclase, are analytical artefacts

resulting powder mounted for analysis by mixing with epoxy. A similar approach was used by Köhler and Brey (1990) to analyse the small amounts of Ca in olivine in equilibrium with Ca-rich clinopyroxene. The Ti content of olivine was then measured only in grains that had been completely isolated from rutile in the epoxy mount.

Selected samples were extracted from the epoxy after electron microprobe analysis for powder X-ray diffraction (XRD). Approximately 25 wt.% of a NIST Si ($a_o = 5.431195$ Å) internal standard was added to each powder. The unit cell volumes were determined using a Siemens D-5005 diffractometer (scintillation counter and Co Kα radiation). The sample mixture was sedimented onto a ''zero background'' quartz plate that was rotated while intensity data were collected from 18 to 135° 2-theta in 0.02° increments taking 9 s per step. Rietveld refinement was carried out using the program DBWS-9807 (Young et al. 1995). R_{Bragg} values for olivine are typically ~5, and for Si, ~2. Titanium-free synthetic fo was also refined under identical conditions.

Experimental results

Results at 1,400 and 1,500°C, 1 bar

Establishing the Ti concentration in olivine

Experimental results are presented in Table 3. Experiments at 1,400 and 1,500°C produced olivine crystals with a diameter of 5–20 μm (Fig. 3a), which are generally homogenous in composition and display straight grain boundaries. Moreover, there was no significant variation in olivine composition throughout a sample, indicating equilibration. The expected paragenesis was found in compositions I, II, IV and V. In composition VI ilmenite failed to appear probably because the addition of Ti-fo shifted the bulk rock composition into a field where only Ti-bearing olivine and pseudobrookite are stable. Ilmenite was also not detected in composition III at 1,500°C. In the silica-rich samples (composition VII) that were expected to produce Ol + Opx + Pbk, a Ti-rich silicate melt formed instead of orthopyroxene. In these samples olivine is much larger (up to 300 μm) and very homogenous (Fig. 3b).

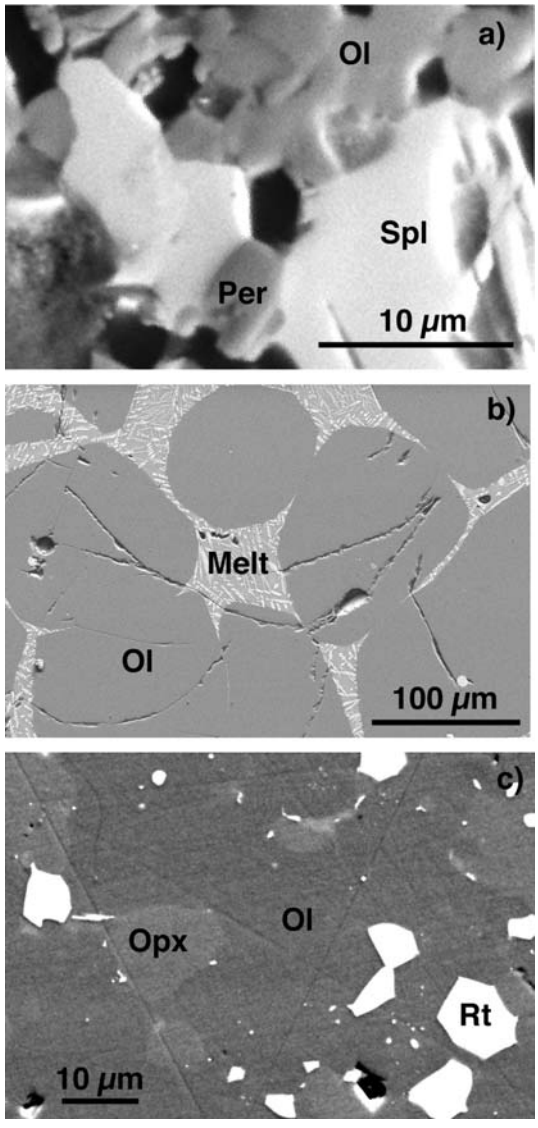

Fig. 3 Back scatter electron images of experimental products. **a** Coexisting olivine (Ol), periclase (Per) and spinel (Spl) (composition I, 1,400°C, 1 atm). **b** Large homogeneous olivine coexisting with a Ti-rich melt containing quench rutile (composition VII, 1,400°C, 1 atm). **c** Equilibrium texture between olivine, orthopyroxene (Opx) and rutile (Rt) at 1,400°C and 15 kbar

The TiO_2 concentrations in olivine for the different parageneses are shown in Fig. 4. Experiments starting with pure forsterite and with the olivine containing 1 wt.% TiO_2 produced within error the same results for compositions I, IV and II, V. The good agreement of these compositional reversals provides evidence that the olivine compositions attained equilibrium. Compositions III and VI (intended paragenesis Ilm + Pbk) were not perfect reversals because minor melt appeared in composition VI (1,500°C) and ilmenite was not always present. The Ti content of olivine from composition III was always higher than that from composition VI. Two sets of experiments, with durations of 5 and 31 days, were run at 1,400°C giving similar results within reasonable experimental uncertainty, indicating that equilibrium was attained. To evaluate whether or not electron scattering and fluorescence was a problem in determining the TiO_2 contents of these olivine crystals, several samples were powdered and mounted in epoxy. All analyses for compositions I, II, IV and V, i.e. the samples with the highest TiO_2 concentrations in olivine, were within error the same as previously determined. However, for compositions III and VI where the Ti content of olivine is lower, the concentrations in the grain mounts were about 0.1–0.2 wt.% below that which had been measured for the coherent samples. For these compositions, the values given in Table 3 derive from analyses of the grain mounts only. Olivine crystals in composition VII were always sufficiently large that phantom Ti contents could be neglected.

Several samples were analysed by XRD to determine the unit cell volume of Ti-bearing olivine. The results show excellent internal consistency between the cell volume and the Ti-content as determined from the electron microprobe analyses (Fig. 5). These data demonstrate that the incorporation of Ti, which has a significantly larger ionic radius than Si, results in a regular increase in the unit cell volume. Therefore, the Ti contents determined by electron microprobe analysis can not be due to submicroscopic inclusions invisible to the SEM, nor are they a phantom analytical artefact due to (for example) the stray electron/fluorescence effect.

The 16 unit cell volumes determined from experiments at 1,400 and 1,500°C and three well equilibrated samples at 1,200°C (compositions I, II and IV) given in Table 3, plus a determination of the volume for pure forsterite of 290.086(5) $Å^3$, were fitted by least squares to a linear relation, to give

$$V(Å^3) = 290.12(1) + 23.67(85)N_{Ti}, \quad (2)$$

where N_{Ti} is Ti(pfu) in olivine. The data were weighted assuming the uncertainties in Ti content given in Table 3, and in unit cell volume of ± 0.02 $Å^3$. This latter uncertainty is slightly larger than that returned from the Rietveld refinements, since the Rietveld method underestimates the uncertainties in lattice parameters due to serial correlation of the XRD data (Post and Bish 1989). With these uncertainties, the reduced chi-squared for the regression was 1.46.

The partial molar volume of the Ti end-member ($N_{Ti} = 1$), which has the formula Mg_2TiO_4, is thus 47.24 ± 0.13 cm^3. By comparison, Mg_2TiO_4 spinel (qd) has a molar volume of 45.29 ± 0.01 cm^3. This accords with the general expectation that the olivine polymorph of AB_2O_4 compounds is generally less dense than the spinel polymorph (Kamb 1968; O'Neill 1998). Clearly the expected effect of pressure would be to decrease the solubility of the Mg_2TiO_4 component in olivine in equilibrium with Mg_2TiO_4-rich spinel.

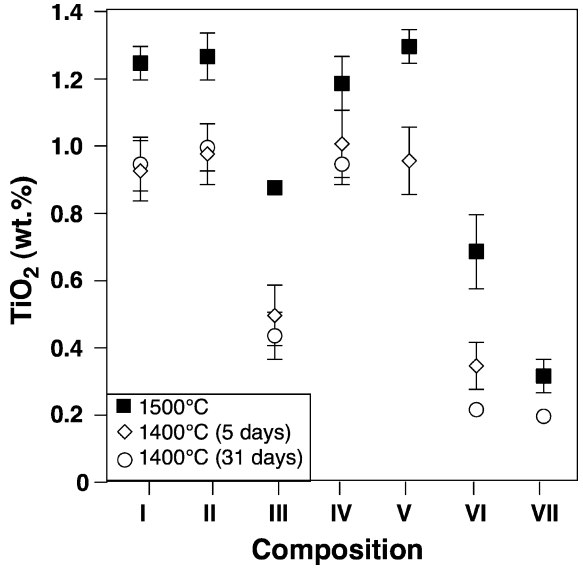

Fig. 4 TiO_2 concentration in olivine at 1,400°C and 1,500°C as a function of bulk rock composition (see Table 2). Note the good agreement between the two series at 1,400°C. Error bars are 1σ for the microprobe analyses

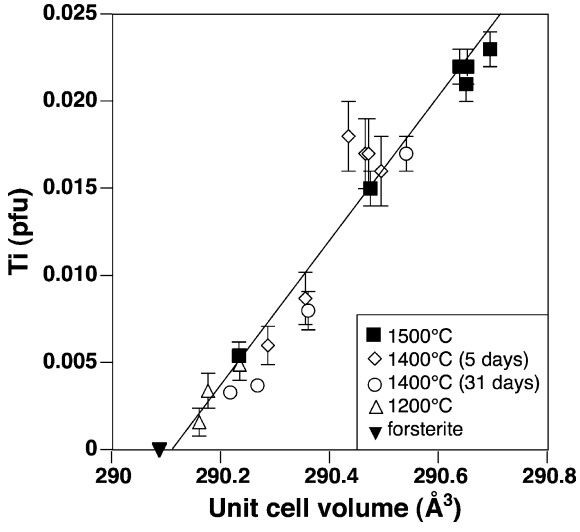

Fig. 5 Variation of unit cell volume as a function of the Ti content of olivine (cations per formula unit). The unit cell volume of forsterite was determined as 290.086 ± 0.005

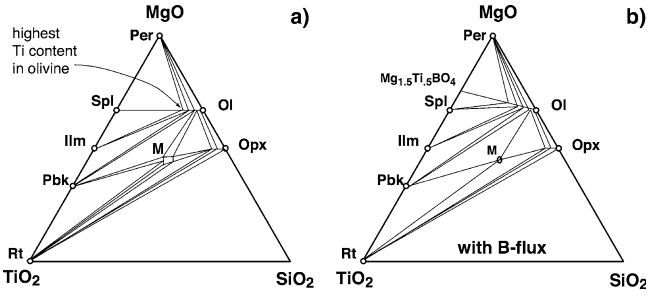

Fig. 6 a Schematic chemography showing the variation in Ti content in olivine as a function of paragenesis. The maximum Ti content is found in parageneses with spinel. **b** Addition of B (from the flux) enhances Ti solubility in olivine and probably produces a Ti–B–olivine

Dependence of Ti solubility in olivine on coexisting phases

The experiments at 1,400 and 1,500°C provide evidence that there is a significant variation in TiO_2 concentration in olivine as a function of paragenesis. The TiO_2 contents are highest when olivine coexists with spinel, regardless of whether the third phase is periclase or ilmenite. Olivine buffered with ilmenite plus pseudobrookite shows significantly lower TiO_2 contents. In samples with the assemblage Ol + Pbk, the Ti content of olivine was slightly lower then when ilmenite was also present. More silica-rich compositions produced pseudobrookite and a Ti-rich silicate melt coexistent with low Ti olivine. This chemography is summarized schematically in Fig. 6a. Orthopyroxene-bearing assemblages were not produced due to the intervention of partial melting. However, the chemography suggests that olivine in equilibrium with orthopyroxene would have a similar but slightly lower TiO_2 content to olivine coexisting with pseudobrookite and a Ti-rich melt.

The observation that a maximum Ti content is achieved with coexisting spinel indicates that Ti substitutes into olivine, at the conditions of these experiments, by a $Mg_2TiO_4 \leftrightarrow Mg_2SiO_4$ exchange, as postulated by O'Neill (1998) for Mn–Fe olivine coexisting with Mn–Fe

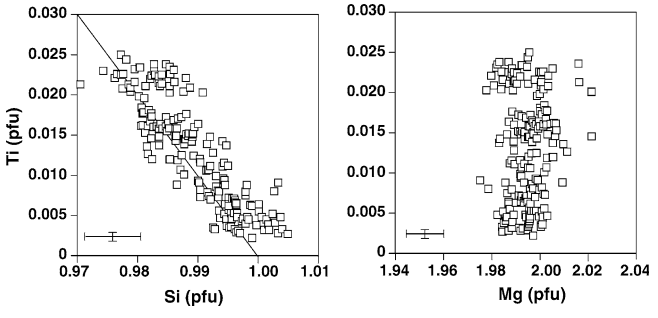

Fig. 7 The negative correlation between Ti and Si and the absence of any correlation between Ti and Mg suggests that Ti substitutes for Si in olivine. Error bars refer to typical analytical 1σ uncertainties of the electron microprobe analyses

ilmenite solid solution. Such an exchange is supported by the electron microprobe analyses which show a clear decrease in Si with increasing Ti (in cations per formula unit (pfu)), with a slope close to −1 (Fig. 7). On the other hand there is no correlation between Ti and Mg. Although the straightforward replacement of Ti for Si on the tetrahedral site to produce the end-member $Mg_2^{[6]}Ti^{[4]}O_4$ is the simplest way of accommodating this substitution, as a general principle stoichiometry can never give site occupancies unambiguously, as any substitution can potentially be accompanied by an order-disorder reaction, such as $Mg^{[6]}Ti^{[6]}Mg^{[4]}O_4$.

Results at 1,200 and 1,300°C, 1 bar

No flux added

In contrast to the higher temperature experiments, a run at 1,300°C for 18 days produced grain sizes of < 5 μm. Moreover, straight grain boundaries were uncommon and there was often significant chemical variation within a single grain as well as from grain to grain. All these observations indicate that the run time was insufficient to achieve equilibrium and these samples are not considered further. A set of samples at 1,200°C, run for 31 days, produced slightly larger grains and textures closer to equilibrium, although there was still significant compositional zoning in the olivine crystals. Because of the small grain sizes, part of this variation could be related to analytical artefacts. For this reason, the samples were ground and mounted as single grains in epoxy. WDS-analyses of all samples yielded reasonable results except for compositions V and VI (Table 3). The Ti concentration of olivine is much lower than at higher temperatures but shows the same dependence on paragenesis. The highest concentration was obtained for samples where olivine coexists with spinel, with all these samples having the same concentration, within error. The lowest value was obtained for composition VII, which contains Ol + Opx + Pbk. To further evaluate these experiments the unit cell volumes of all samples were determined (Table 3). Olivine from compositions II and V have the largest cell values, compositions III and VI intermediate, and composition VII the smallest value, in agreement with the relationship established at higher temperature. Microprobe analysis indicates that composition I contains forsterite that did not react and therefore the average unit cell volume is lower than expected. Similarly there is unequilibrated high-Ti olivine remaining in composition IV resulting in a larger average cell volume. The reversal samples from compositions II and V have identical average values and are probably close to equilibrium. The unit cell volume is, within error, equal to that of the olivine produced in composition VII at 1,500°C, which contains 0.31 wt.% TiO_2. Hence, the average composition of olivine in compositions II and V at 1,200°C must be the same. In fact, the measured Ti content of olivine from composition II is

0.27 ± 0.05 wt.% TiO_2, within error equal to the value obtained from the unit cell volume.

Using different fluxes

Since the presence of melt was observed to strongly enhance olivine growth, the effect of adding various fluxes was also investigated. Compositions I, II, III and VII were mixed with 10% of a diopside–anorthite eutectic melt composition and equilibrated at 1,300°C. The addition of this silica-rich melt resulted in the consumption of MgO and a shift in the average bulk composition. Composition I did not produce an equilibrium assemblage. Composition II produced homogenous 20–80 μm olivine crystals coexisting with pseudobrookite and melt (Table 3). For compositions III and VII the Ti phases were consumed into the melt.

For the next attempt, 10% of a K_2O–Na_2O flux (molar proportion 1:1), obtained from decarbonatisation of K- and Na-carbonate was added to four compositions, with three yielding reasonable results (Table 3). In particular, the Ti content of olivine coexisting with pseudobrookite and melt was similar to that of samples produced using the diopside–anorthite eutectic flux. However, the variation in olivine composition for I was higher than desirable and thus a third flux was tested; 10% sodium-tetraborate was added to the same four compositions and run at 1,200°C for 7 days. The resulting samples contained small amounts of melt and the phases displayed equilibrium textures. Olivine crystals were sufficiently large (10–40 μm) to be analysed by both SEM-EDS and WDS with confidence. However, the results were significantly different from those of the non-flux grown crystals. First, the highest Ti concentration in olivine was obtained for composition I but not for composition II. Second, the maximum Ti-content of olivine in composition I was about four times higher than that in the corresponding run without flux. This suggests that the presence of B might enhance Ti solubility in olivine. The difference in the solubilities of Ti in olivine between the parageneses Ol + Spl + Per and Ol + Spl + Ilm suggests that the composition of the olivine in the B-containing system lies on the join Mg_2SiO_4—$Mg_{1.5}Ti_{0.5}BO_4$ (Fig. 6b). Hence we suggest that there is a coupled substitution $Ti^{[6]}_{0.5}B^{[4]}$ $Mg^{[6]}_{-0.5}Si^{[4]}_{-1}$ in which Ti substitutes for Mg on the octahedral site, with charge-balance maintained by substitution of B for Si on the tetrahedral site. This result is potentially of importance as it shows that under certain circumstance Ti may substitute into olivine by a mechanism which does not have the M_2TiO_4 stoichiometry. Interestingly, the cathodoluminescence colour of olivine caused by the microprobe electron beam was brown in the samples prepared with the B flux whereas in all other experiments it was blue. This indicates that the cathodoluminescence of olivine might be sensitive to whether Ti is incorporated into an octahedral or a tetrahedral site.

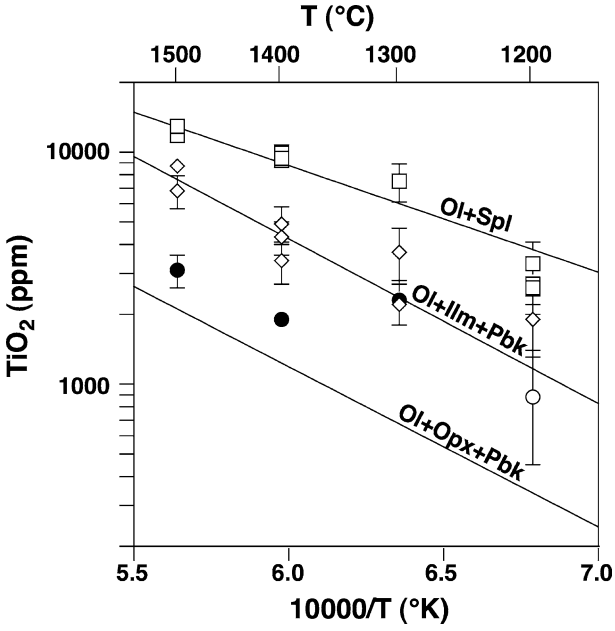

Fig. 8 Variation of TiO_2 contents of olivine as a function of temperature and composition. Olivine coexisting with Spl (squares), with Pbk (diamonds) and either with Opx + Pbk (open circle) or M + Pbk (filled circles) are shown. The trend lines were calculated from a thermodynamic analysis of the data (see text for discussion)

Temperature dependence

The results from 1,500 to 1,200°C demonstrate a strong decrease in the solubility of Ti in olivine with decreasing temperature (Table 3). As shown above, olivine buffered by spinel displays the highest TiO_2 content. These runs exhibit a linear relationship between log TiO_2 and 1/T (Fig. 8). Similar trends were found for the Ti contents of olivine coexisting with Ilm and Pbk, which compare very well with the predicted trends from the thermodynamic analysis based on the Ol + Spl data (see below). It is not possible to constrain directly the trend for the paragenesis Ol + Opx + Ti-phase, because orthopyroxene was only found at 1,200°C. The phase relations (Fig. 6) show that the TiO_2 content of olivine coexisting with orthopyroxene must be slightly lower than that of olivine coexisting with melt. This agrees well with the thermodynamically calculated trend, which predicts the TiO_2 content of olivine coexisting with Opx + Pbk to be lower

Table 4 Piston cylinder experiments at 1,400°C (all for 48 h) and TiO_2 contents of synthesised olivine and orthopyroxene (wt.%)

Run	P (kbar)	Phases	TiO_2 (Ol)	TiO_2 (Opx)
C-1227	15	Ol + Opx + Rt	0.178(15)	1.54(4)
C-1230	25	Ol + Opx + Rt	0.209(25)	1.30(7)
C-1234	35	Ol + Opx + Rt	0.191(19)	1.16(3)
UHP 141	45	Ol + Opx + Rt	0.194(47)	1.09(4)
UHP 142	55	Ol + Opx + Rt	0.234(18)	1.11(4)

than that measured in the paragenesis with Pbk + M (Fig. 8).

Pressure dependence

To evaluate the pressure dependence of Ti solubility in olivine, piston cylinder experiments were undertaken at 1,400°C and 15, 25, 35, 45 and 55 kbar (Table 4). The starting material was an oxide mix consisting of 15% rt, 25% en and 60% fo. The run products were mounted in epoxy as both chunks, to investigate the phase and textural relations, and as single grains. In all runs Ol + Opx + Rt were obtained in agreement with earlier work (MacGregor 1969), showing that at ~1,400°C and $P > 14$ kbar, rutile is the stable phase together with Ol + Opx (Reaction 1).

The experiments displayed well-equilibrated textures (Fig. 3c). The average grain size decreases with increasing pressure from about 20 to 10 μm. All olivine grains were analysed by WDS on a Cameca SX-100. Careful analyses of olivine synthesised at 15 kbar showed that it is not trivial to determine the TiO_2 content of crystals coexisting with rutile in such fine-grained samples. The TiO_2 content of olivine in the mounted chunks displayed considerable compositional variation. If only data obtained from the centre of large crystals is considered, the average TiO_2 content is about 0.26 wt.% (Fig. 9a). However, profiles from rutile grains into the centre of these large crystals reveal a decrease in the TiO_2 content from rim to core, corresponding to "phantom Ti contents" (e.g. Fig. 2) which never reach a constant value. Hence it is likely that the concentrations obtained from the cores of large crystals are still too high. Profiles through isolated olivine grains at the end of the capsule yield a much more constant TiO_2 content of 0.18 wt.%. For more accurate measurements, the physically separated olivine crystals were analysed as grain mounts to minimise the effect of electron scattering and fluorescence. The average TiO_2 content of olivine measured in this way is within error identical to the plateau value of the grains isolated from rutile at the end of the capsule, but significantly lower than that obtained from the cores of olivine in close contact with rutile (Fig. 9a). Fig. 9b shows the TiO_2 content of olivine for the pressure series from 15 to 55 kbar. The analyses of the grain mounts, which provide the true TiO_2 content, do not display a clear trend and scatter slightly around 0.2 wt.% TiO_2, indicating that there is no significant increase in TiO_2 with pressure. In contrast, the TiO_2 content of olivine determined from cores of crystals for samples in which the textural relationship with rutile is preserved, display an apparent increase between 35 and 55 kbar. We suggest that this trend is an artefact due to the decrease in grain size with increasing pressure, which inevitably causes an increase in the contribution of TiO_2 from scattered electrons and fluorescence.

Surprisingly, the Ti concentration in orthopyroxene was very high in this Al-free system (Table 4). The orthopyroxene contained 1.5 wt.% at 15 kbar, 1.16 wt.% at 35 kbar, and a constant value of ~1.1 wt.% at 45 and 55 kbar. Similarly to olivine, there is a negative correlation between Si and the number of Ti cations per formula unit. Although in natural, compositionally complex pyroxene solid solutions it is usually assumed that Ti occurs in octahedral coordination, charge-balanced by Al substituting for Si in the tetrahedral sites (e.g., as in the end-members $CaTiAl_2O_6$, $MgTiAl_2O_6$ or $NaTiAlSiO_6$), the present results show that straightforward substitution of Ti (presumably in the tetrahedral site) for Si may also be petrologically significant at high temperatures.

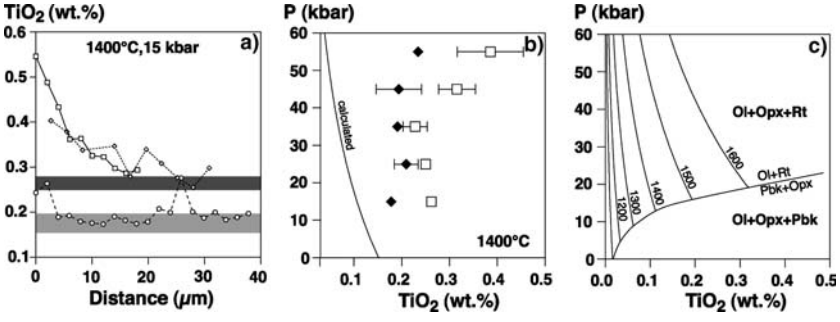

Fig. 9 **a** Profiles from edge (0 μm) to centre of olivine crystals retrieved from the experiment at 15 kbar and 1,400°C. Most olivine crystals (*squares*, *diamonds*) display a decrease in TiO_2 content from rim to core and there is no plateau composition. The dark grey bar represents the average composition of the olivine cores. The light grey bar corresponds to the Ti content of physically separated crystals. Core analyses are therefore affected by the scatter electron effect (see Fig. 2) and significantly overestimate the actual TiO_2 content. A few isolated olivine crystals (*circles*) at the edge of the capsule display a plateau composition, which is within error identical to the correct value. **b** Ti-contents of olivine synthesised at 1,400°C and 15 to 55 kbar determined from separated crystals (*filled diamonds*) and from olivine remaining in contact with rutile and orthopyroxene (*open squares*). The line represents calculated values of TiO_2 in olivine according to the thermodynamic model given in the discussion. **c** Calculated TiO_2 contents of olivine coexistent with Opx + Rt as a function of pressure and temperature. Note that in all cases the Ti solubility decreases with increasing pressure

Thermodynamic analysis

By extracting the thermodynamic properties of the Mg_2TiO_4 component in olivine, we aim firstly to

demonstrate internal consistency in our experimental results. We can then use the thermodynamic analysis to compute trends in the Ti content of olivine in naturally occurring mineral assemblages as a function of temperature and pressure, in order to understand the petrological significance of the observed Ti exsolution.

The amount of Ti in olivine dissolved as the component Mg_2TiO_4 is given by the reaction

$$\underset{\text{Olivine}}{Mg_2TiO_4} = \underset{\text{Spinel}}{Mg_2TiO_4} \quad (3)$$

For small amounts of Ti we assume that the Mg_2TiO_4 (ol) component is in its Henry's law region, hence at equilibrium

$$\begin{aligned} RT \ln X^{\text{ol}}_{Mg_2TiO_4} &= -\Delta_r G^{\text{o}}_{(T,1\text{ bar})}(3) - RT \ln \gamma^{\text{ol},\infty}_{Mg_2TiO_4} \\ &= -\Delta_r G^{*}_{(T,1\text{ bar})} \end{aligned} \quad (4)$$

where $\Delta_r G^{*}_{(T,1\text{ bar})}(4)$is the free energy of reaction in which Mg_2TiO_4 (ol) is referenced to a standard state of infinite dilution in Mg_2SiO_4 olivine at the pressure and temperature of interest. The mole fraction $X^{\text{ol}}_{Mg_2TiO_4}$ is equivalent to N_{Ti}, and the spinel is assumed to be pure stoichiometric Mg_2TiO_4 (qd).

By fitting the 14 values of N_{Ti} in Table 3 for olivine coexisting with spinel (qd) at 1,200–1,500°C to Eq. 3, we obtain

$$\Delta_r G^{*}_{(T,1\text{ bar})}(4) = -88195 + 18.25\,T(\text{J mol}^{-1}) \quad (5)$$

The value of χ^2_ν for the regression is 1.15, indicating a good fit. The free energy of formation of Mg_2TiO_4 olivine from the elements in this standard state is then given by

$$\begin{aligned} \Delta_f G^{*}_{(T,1\text{ bar})}(Mg_2TiO_4, \text{ol}) = \Delta_f G^{\text{o}}_{(T,1\text{ bar})}(\text{qd}) + 88195 \\ - 18.25\,T(\text{J mol}^{-1}) \end{aligned} \quad (6)$$

The free energy of formation of qd (Table 5) is taken from O'Neill and Scott (in press), and is in a form that is compatible with the thermodynamic database of Holland and Powell (1998). Therefore this database will be used as the source for other endmembers except karrooite ($MgTi_2O_5$), which is not treated. For this endmember we have used the recommended values of Chatterjee et al. (1998) at 1 bar, adjusting the entropy and enthalpy of formation slightly to make the data compatible with the Holland and Powell data for other phases, and the known phase relations of ko in the system MgO–TiO_2–SiO_2 at atmospheric pressure, as recently summarised by Xirouchakis et al. (2002).

We tried using the more comprehensive thermodynamic model of Xirouchakis et al. (2002) for ko, which treats the order–disorder of Mg and Ti explicitly, but this returns values for the free energy of formation that are too negative to be compatible with the Holland and Powell database for the three reactions: gk + rt = ko, fo + rt = ko + en, and en + rt = ko + SiO_2. While it was possible to make an empirical adjustment to the enthalpy of formation of ko given by Xirouchakis et al. (2002) of about +7.5 kJ mol^{-1} to fit these reactions, this adjusted value then implies that gk would break down to ko + qd (3 $MgTiO_3 = MgTi_2O_5 + Mg_2TiO_4$) at ~1,600 K, contrary to many observations of the stability of gk at high temperatures; for example, Woerman et al. (1969) determined that gk melts incongruently to qd + liquid at 1,630°C. This implies that the non-configurational entropy of ordered ko has been overestimated by Xirouchakis et al. (2002). Their value of 149.55 J K^{-1} mol^{-1} at 298 K is much larger than that measured calorimetrically, which is 127.2 ± 0.8 J K^{-1} mol^{-1} (Todd 1952). The difference of 22.35 J K^{-1} mol^{-1} is larger than the maximum configurational entropy of completely disordered ko (15.9 J K^{-1} mol^{-1}). The value adopted here, 134.5 J K^{-1} mol^{-1}, when compared to the calorimetric value of Todd (1952), implies a configurational contribution of 7.3 J K^{-1} mol^{-1}, which corresponds to a quenched-in degree of disorder that is the equilibrium disorder at ~550°C, according to the order–disorder model of Xirouchakis et al. (2002). Our adopted thermodynamic data for ko (Table 5) are consistent with gk being stable to its melting point.

The amount of Ti in olivine in other parageneses can now be calculated as follows. For the paragenesis Ol + Ilm + Pbk, the controlling reaction is:

$$Mg_2TiO_4 + MgTi_2O_5 = 3MgTiO_3 \quad (7)$$

From the thermodynamic data for qd and ko in Table 5, plus that for Mg_2SiO_4 (ol) and gk from Holland and Powell (1998), we obtain

Table 5 Thermodynamic data

Phase	$\Delta_f H^{\circ}_{(298\text{ K},1\text{ bar})}$	$S^{\circ}_{(298\text{ K},1\text{ bar})}$	$C_p = a + bT + cT^{-2} + dT^{-1/2}$ (in J K^{-1} mol^{-1})				$V^{\circ}_{(298\text{ K},1\text{ bar})}$ (J bar^{-1})	α° (K^{-1})	κ (kbar)
			a	b (×10^2)	c	d			
Mg_2TiO_4 (qd)	−2157.41	111.2	161.7	.03286	−2382200	−278.6	4.529	5.48	1890
$MgTi_2O_5$ (ko)	−2503. 20	134.5	271.04	-	−716690	−2015.8	-	-	-

Mg_2TiO_4 from O'Neill and Scott (submitted) and $MgTi_2O_5$ from Chatterjee et al. (1998), modified for compatibility with Holland and Powell as described in the text. Data for all other substances used in this work are from Holland and Powell (1998)

$$\Delta_r G^*_{(T,1\,\mathrm{bar})}(7) = -112813 - 79.63\,T + 14.365\,T\ln T\,(\mathrm{J\,mol^{-1}}) \quad (8)$$

Similarly for the paragenesis Ol + Pbk + Opx

$$\underset{\text{Olivine}}{Mg_2TiO_4} + 0.75\underset{\text{Orthopyroxene}}{Mg_2Si_2O_6} = 0.5\underset{\text{Pseudobrookite}}{MgTi_2O_5} + 1.5\underset{\text{Olivine}}{Mg_2SiO_4} \quad (9)$$

$$\Delta_r G^*_{(T,1\,\mathrm{bar})}(9) = -114290 - 65.16\,T + 11.112\,T\ln T\,(\mathrm{J\,mol^{-1}}) \quad (10)$$

The amounts of Ti in ol in ppm calculated from these equations are compared to our experimental data in Fig. 8. The calculated Ti content can also be extrapolated to lower temperatures. It is remarkable how well this thermodynamic model fits the experiments containing Ol + Ilm + Pbk; at 1,400°C the model predicts 0.44 wt.% TiO_2 in olivine whereas in the two experiments with this assemblage the measured values were 0.43 and 0.49 wt.% TiO_2. Also the thermodynamic model allows reaction (9) to be assessed which could not be directly evaluated experimentally.

Ti in olivine at high pressures

At higher pressures Ol becomes stable with Rt according to reaction (1), hence the solubility of Ti in olivine as the Mg_2TiO_4 component is given by

$$\underset{\text{Olivine}}{Mg_2TiO_4} + \underset{\text{Orthopyroxene}}{Mg_2Si_2O_6} = \underset{\text{Rutile}}{TiO_2} + 2\underset{\text{Olivine}}{Mg_2SiO_4}$$

Using our value for the partial molar volume of Mg_2TiO_4 (Ol) of 47.24 ± 0.13 cm^3, the change in molar volume for this reaction at 298 K and 1 bar ($\Delta_r V^{\circ}_{(298\ \mathrm{K},1\ \mathrm{bar})}$) is -3.72 cm^3, which is a decrease of about 4%. Clearly the amount of the Mg_2TiO_4 component in olivine should decrease with increasing pressure. This is illustrated in Fig. 9c, where we have used our thermodynamic model to plot calculated values of wt.% TiO_2 in olivine for temperatures at 100°C intervals from 1,000 to 1,600°C, and pressures from 15 to 55 kbar. We used the form of the equation of state recommended by Holland and Powell (1998), and assumed that the thermal expansion parameter and bulk modulus of Mg_2TiO_4 (Ol) was the same as that for qd (Table 5). The calculation is not sensitive to these two parameters and substituting the values for fo makes negligible difference.

The experimentally measured TiO_2 content of Ol in the paragenesis Ol + Opx + Rt at 1,400°C is 0.2 wt.%, independent of pressure from 15 to 55 kbar. This is clearly more than our calculated values. This may be because the experimentally determined TiO_2 content includes (despite our best efforts) a contribution from rutile, or from Ti substituting in a form other than the Mg_2TiO_4 component.

Discussion

We first compare the results of our study on the Ti content in olivine as a function of composition, pressure and temperature to previous experimental work. Then the Ti contents of natural olivine from spinel and garnet peridotites are compiled. A comparison of this data with the experimental results allows the conditions at which Ti saturation occurs in anhydrous natural olivine to be determined. It also allows the importance of Ti incorporation as a hydrous $MgTiO_2(OH)_2$ defect to be determined, and how different incorporation mechanisms may influence the nature of the exsolved Ti-phase.

Experimental constraints on Ti solubility in olivine

Our experiments demonstrate that there is a strong compositional control on the solubility of Ti in olivine. At atmospheric pressure, the solubility drops by about a factor of four from olivine coexisting with spinel to olivine coexisting with melt/orthopyroxene + pseudobrookite (Fig. 4). While mantle olivine is generally buffered with orthopyroxene, appropriate buffering has not always been achieved in previous experimental studies. Gudfinnson and Wood (1998) used a two-phase assemblage of olivine + a Ti-phase; in these experiments, small variations in the Mg/Si ratio of the starting material could produce either additional spinel or orthopyroxene, which strongly influences the Ti solubility. Ulmer et al. (1998) used a olivine + ilmenite starting assemblage that produced Ol + Ilm + Rt below 40 kbar, Ol + Opx + Rt from 40 to 75 kbar and Ol + Opx + Ilm at 90 kbar (P. Ulmer 2004, personal communication). This change in paragenesis might produce small variations in the Ti contents of olivine. Tinker and Lesher (2001) stated that they had determined the maximum solubility of Ti in olivine because their experiments were buffered with rutile. However, the chemography shows that the maximum Ti content is achieved when olivine is buffered by spinel (Fig. 6a). Experiments in more complex systems containing Al, Na and Ca, giving rise to the paragenesis Ol + Opx + Ti-rich melt, produced olivine with ~0.2 wt.% TiO_2 at 12 kbar, 1,360°C and 28 kbar, 1,530°C (Xirouchakis et al. 2001). The results at 1,530°C are very similar to our calculated values in the paragenesis Ol + Opx + Rt at 28 kbar (Fig. 9c). This is in agreement with the phase relations determined, which indicate that there is little difference in the Ti-content of olivine coexisting with orthopyroxene and either a Ti-phase or a Ti-rich melt (Fig. 6a). In such complex systems, other Ti substitutions in olivine are likely to occur, especially Ti incorporation on the octahedral site, coupled with the substitution of Al for Si on the tetrahedral site to maintain charge-balance, similar to our observation in the system containing B. This may explain the higher

TiO_2 content of the experiments at 1,360°C, 12 kbar compared to that predicted by our model.

There is general agreement among all the experimental studies that the Ti content of olivine increases with increasing temperature, however, the absolute values differ markedly. Ulmer et al. (1998) reported 0.105 wt.% TiO_2 at 1,200°C and 0.135 wt.% TiO_2 at 1,400°C in the paragenesis Olivine (Fo_{90}) + Orthopyroxene + Rutile + water at 40–75 kbar. The latter value is slightly lower than the ~0.2 wt.% TiO_2 in olivine we found in the Fe free, nominally anhydrous system coexisting with enstatite and rutile, but still higher than the calculated values. This suggests that in the hydrous experiments Ti solubility may be increased by the presence of Ti-clinohumite type defects. Dobrzhinetskaya et al. (1999) found an increase in the TiO_2 content of olivine in an anhydrous system from 0.50 wt.% at 1,177°C to 1.12 wt.% at 1,427°C and 120 kbar. These values are over an order of magnitude higher than predicted by the thermodynamic model derived in the present study. One possible explanation for this discrepancy might be the design of the assembly used by Dobrzhinetskaya et al. (1999). In these experiments the Opx-bearing starting material was contained in a MgO capsule, possibly resulting in the consumption of orthopyroxene to produce olivine. The paragenesis after the run was not reported and it is highly likely that the experiments were actually buffered by periclase, which strongly increases the capability of olivine to incorporate Ti.

The most controversial argument concerns the pressure dependence of the Ti solubility. Dobrzhinetskaya et al. (1999) and Tinker and Lesher (2001) reported a significant increase in the TiO_2 content with pressure on the basis of anhydrous experiments. Our data show an apparent increase in Ti content when Ti was analysed within the mounted chunks due to the phantom Ti effect. When the olivine grains were separated, no increase in Ti content with pressure was observed (Fig. 9b). This is consistent with data from hydrous experiments by Ulmer et al. (1998), which found no pressure dependence on the Ti solubility in olivine from 10 to 100 kbar. The grain size in their experiments was >150 μm and hence the reported values are likely to represent the true solubility. The 0.07 wt.% TiO_2 content of olivine coexisting with ilmenite determined by Gudfinnson and Wood (1998) at 1,400°C and 140 kbar, is in good agreement with the value of Ulmer et al. (1998), but much lower than the value of 1.12 wt.% proposed by Dobrzhinetskaya et al. (1999) at 1,427°C and 120 kbar. O'Neill (1998) demonstrated a decrease in the TiO_2 content of Fe–Mn olivine with pressure between 1 bar and 25 kbar, and pointed out that such a decrease was expected if the Ti substitution in the olivine has the M_2TiO_4 stoichiometry. Our experiments from 15 to 55 kbar produce, within error, constant Ti contents in olivine. Additionally, our thermodynamic analysis suggests that in the water–free system Ti contents decrease with increasing pressure. Hence our new data on the anhydrous system combined with the results from Ulmer et al. (1998) on the hydrous system, do not support the hypothesis that Ti-rich olivine can be used as a tracer for an ultra-deep origin of certain orogenic peridotites.

Table 6 Calculated TiO_2 contents of mantle minerals on the basis of modal abundances (calculated from major element composition), bulk rock TiO_2 contents and mineral partitioning

Rock type	Hot garnet peridotite		Cold garnet peridotite			Spinel peridotite	
	lherz.	harz.	lherz.	harz.	A.A.	lherz.	harz.
Modal abundance (%)							
Ol	50	65	50	65	55	48	70
Cpx	10	7	10	7	10	21	10
Opx	22	19	22	19	20	29	19
Gnt	18	9	18	9	15		
Spl						1	1
Partitioning							
Cpx/Ol (Ti)	12.7	12.7	9	9	9	45	60
Opx/Ol (Ti)	7.8	7.8	4.5	4.5	4.5	16	24
Gnt/Ol (Ti)	34	34	10.8	10.8	10.8		
Spl/Ol (Ti)						24	33
TiO_2-content (wt.%) contents							
Bulk rock	0.200	0.083	0.200	0.083	0.13	0.206	0.083
Ol	0.021	0.014	0.046	0.027	0.033	0.014	0.007
Cpx	0.264	0.173	0.415	0.24	0.295	0.626	0.43
Opx	0.162	0.106	0.208	0.12	0.147	0.223	0.172
Gnt	0.708	0.464	0.498	0.289	0.354		
Spl						0.334	0.236

Partitioning data for "hot garnet peridotites" ($T > 1{,}150$°C) and "cold garnet peridotites" ($T < 1{,}150$°C) are from Hervig et al. (1986) and for spinel peridotite are from McDonough et al. (1992). Bulk rock data are from McDonough et al. (1992) for harzburgite (harz.) and spinel peridotite lherzolite (lherz.), Sun and McDonough (1989) for garnet peridotite lherzolite (pyrolite composition) and Risold (2001) for the Alpe Arami (A.A.) garnet peridotite. Additional abbreviations not given in Table 1: *Cpx* Clinopyroxene, *Gnt* Garnet

TiO_2 contents of mantle olivine

An extensive compilation of olivine compositions from mantle xenoliths shows that olivine from garnet peridotites generally displays higher TiO_2 contents (mostly 100–200 ppm) than olivine from spinel peridotites (< 70 ppm), with the highest TiO_2 content of olivine from garnet peridotites reaching ~450 ppm (Hervig et al. 1986). McDonough et al. (1992) showed that in the spinel peridotite field, the TiO_2 content of olivine is strongly dependent on bulk rock composition. In a fertile peridotite, olivine contains 110 ppm TiO_2, whereas in more depleted rocks TiO_2 ranges from 40 to 70 ppm. The measured TiO_2 content of olivine containing ilmenite inclusions from the Alpe Arami garnet peridotite reaches ~330–350 ppm (Hacker et al. 1997; Reusser et al. 1998), within the range of values for olivine from garnet peridotite xenoliths (Hervig et al. 1986).

With the exception of rare ilmenite-bearing garnet peridotites from kimberlites (Boyd and Nixon 1978), there is generally no free Ti-phase present in mantle assemblages and consequently TiO_2 in mantle minerals is below the saturation level given by the appropriate paragenesis. The Ti content of olivine is then determined by Ti partitioning between all mantle phases, i.e., by bulk rock TiO_2 content, the modal abundances of the different phases and their Ti partitioning. Table 6 displays calculated TiO_2 contents of mantle phases for fertile (lherzolite) and depleted mantle (harzburgite) compositions on the basis of the calculated mineral abundances and published Ti partitioning data. The results demonstrate that the highest olivine TiO_2 contents of ~460 ppm are obtained in fertile, cold garnet lherzolites (T < 1,150°C) whereas olivine from spinel peridotites have significantly lower concentrations. The decrease in pyroxene/olivine Ti partitioning from spinel to garnet peridotite might be explained by changes in the pyroxene major element composition. Ti in pyroxenes is at least partly incorporated by the exchange $Ti^{[6]}\ Al_2^{[4]}\ Mg^{[6]}{}_{-1}Si^{[4]}{}_{-2}$ and thus the Ti in pyroxenes is likely to be linked to their Al_2O_3 content. Accordingly, pyroxene/olivine Ti partitioning is expected to be lowest where the Al_2O_3 content of pyroxene is lowest; pyroxenes in the garnet peridotite field have Al_2O_3 contents of 0.5–2.5 wt.%, compared to 4–8 wt.% in the spinel peridotite field. In fact, the value for Opx/Ol Ti partitioning of 4.5 in "cold garnet peridotites" is close to the value of ~5.5 determined in this study for our simple Al-free system at 35–55 kbar and 1,400°C (Table 4).

The approach described above can be used to calculate the theoretical TiO_2 concentration of olivine from the Alpe Arami peridotite using the cold garnet lherzolite partitioning data and the bulk rock data given by Risold (2001). The 0.13 wt.% TiO_2 in the bulk rock translates into 330 ppm TiO_2 in olivine (Table 6), which is exactly the same value as determined by microprobe (Hacker et al. 1997) and laser-ablation ICP-MS (Reusser et al. 1998) analyses. Reports of TiO_2 contents of 0.5–1 wt.% in some Alpe Arami olivine (Dobrzhinetskaya et al. 1996; Green et al. 1997; Bozhilov et al. 2003) are hard to reconcile with the whole rock and partitioning data. The Alpe Arami peridotite contains about 55–60% olivine and noting that garnet and pyroxenes always contain more TiO_2 than olivine, the bulk rock TiO_2 contents would need to be above 1 wt.% if the olivine was to have had such high TiO_2 concentrations. However, the Alpe Arami peridotite only contains 0.13 wt.% TiO_2 and therefore high Ti-olivine, if real, cannot represent equilibrium concentrations. Hence, such "non equilibrium" concentrations should not be used to speculate on ultra-deep formation conditions for the Alpe Arami peridotite.

Possible mechanisms of Ti-phase exsolution

Before applying our results to natural systems, we need first to consider the effects of Fe^{2+}. Preliminary data on the system MgO–FeO–TiO_2–SiO_2 (Pownceby and O'Neill, unpublished) plus the observations of O'Neill (1998) show that the effect of increasing Fe^{2+} in $(Mg,Fe)_2SiO_4$ olivine is to increase the amount of TiO_2 that dissolves in olivine in equilibrium with $(Mg,Fe)_2TiO_4$ spinel at constant temperature and pressure. However, the effect is sufficiently small that it may be neglected for upper mantle compositions with molar Mg/(Mg + Fe) ~0.9. Experiments show that the solubility of Ti in olivine is strongly dependent on composition and temperature but not pressure. The olivine in typical mantle peridotitic compositions coexists with orthopyroxene along any realistic geotherm to ~70 kbar. Thus it is unlikely that changes in the buffering assemblage lead to the observed exsolution of Ti-phases. Our experimental results and the thermodynamic analysis suggests that Ti saturation in olivine can result from cooling. The calculated trend of decreasing TiO_2 content with decreasing temperature in the paragenesis Ol + Opx + Rt can be combined with the TiO_2 contents of mantle olivine to evaluate the temperature at which saturation is reached (Fig. 10). Olivine from spinel peridotites generally have TiO_2 contents lower than 100 ppm and consequently saturation in an anhydrous system is reached at temperatures below 1,050°C. Olivine from garnet peridotites typically contain higher TiO_2 contents of ~100–400 ppm (Hervig et al. 1986), and hence they reach the saturation level at higher temperatures, ~1,100–1,300°C. The presented data suggest that slow cooling without complete recrystallisation of olivine is a feasible mechanism to explain exsolution of Ti-rich phases. The results of this study show that Ti substitutes for Si as the component M_2TiO_4 in olivine under anhydrous conditions. Hence, such slow cooling should produce spinel exsolution in olivine. The presence of ilmenite rods in some olivine suggests that there is an additional mechanism, or component, of Ti incorporation. It is worth noting that the highest TiO_2 contents in olivine, ~300–450 ppm, are reported from "cold garnet peridotite" xenoliths ($T \leq 1{,}150$°C) (Hervig

et al. 1986). Such high concentrations at relatively low temperatures are beyond the anhydrous saturation level. We therefore suggest that these olivine crystals might contain significant amounts of Ti located on an octahedral site either as Ti-clinohumite defects or charge balanced by other trace elements such as Al, B, Na or Li. Occasionally, olivine is buffered by a titanium phase in mantle xenoliths from kimberlites that have experienced metasomatism by a Ti-rich liquid. As an example, Jones et al. (1982) describe recrystallised olivine in harzburgites coexistent with rutile that contain 500 ppm TiO_2, which formed at 1,000–1,100°C (Boyd and Nixon 1978). Again this value is higher than that required for saturation in a dry Ol + Opx + Rt paragenesis (Fig. 10) suggesting the presence of an additional Ti component.

Temperature estimates for Alpe Arami derived from core mineral compositions indicate an early high temperature stage of ~1,150°C (Paquin and Altherr 2001). The olivine would have contained ~350 ppm TiO_2 prior to exsolution, which is above the anhydrous saturation level and hence it is likely that some Ti was present on an octahedral site. The main equilibration temperature of Alpe Arami garnet peridotite is ~840°C (Nimis and Trommsdorff 2001) which would favour the significant Ti exsolution observed. Ilmenite rods are only found in this texturally oldest olivine generation whereas younger olivine neoblasts are free of exsolutions (Green et al. 1997; Risold 2001). The TiO_2 content of the younger olivine is about 60 ppm (Reusser et al. 1998), well above the expected saturation level at 840°C (Fig 10). However, the absence of ilmenite exsolution is attributed to the presence of Ti-clinohumite defects as indicated by Fourier-Transformed-Infra-Red spectroscopy, which showed significant H_2O in olivine and provided direct evidence for this type of Ti substitution (own unpublished data). Hence the 60 ppm represents the total Ti incorporated as both anhydrous (Mg_2TiO_4) and hydrous ($MgTiO_2(OH)_2$) components at 840°C. If the Ti-phase exsolution is only related to saturation of the anhydrous Ti component in olivine, the exsolved Ti-phase would be expected to have spinel stoichiometry. The fact that exsolution produces ilmenite suggests that the hydrous Ti component in olivine forms the rods by the reaction $MgTiO_2(OH)_2 => MgTiO_3 + H_2O$. This hypothesis was first proposed by Risold et al. (2001) on the basis of optical observations and transmission electron microscopy. They found that ilmenite is sometimes aligned in planes consistent with the prograde breakdown of clinohumite lamellae in olivine. However, Risold et al (2001) did not explain the origin of the clinohumite layers. Ti-clinohumite has the formula $4(Mg_2SiO_4)Mg_{1-x}Ti_x(OH)_{2-2x}O_{2x}$ ($X \leq 0.5$), which represents an olivine unit plus a hydrous, titaniferous interlayer. The Mg_2TiO_4 component in olivine may react with water to form a Ti-clinohumite like defect. Metamorphism beyond the stability of these Ti-clinohumite defects can result in their partial breakdown to olivine + ilmenite rods + water (eg. Risold et al, 2001). In such a scenario, the formation of ilmenite rods in olivine is likely to be a multistage process involving: (a) formation of Ti-rich olivine in the garnet-peridotite field; (b) cooling and partial hydration to form Ti-clinohumite defects during exhumation; and (c) subduction and prograde metamorphism leading to the break down of the Ti-clinohumite defects and concomitant formation of ilmenite rods. Such a multistage evolution has been proposed for many Alpine peridotites on the basis of other geological evidence (Trommsdorff et al. 2000).

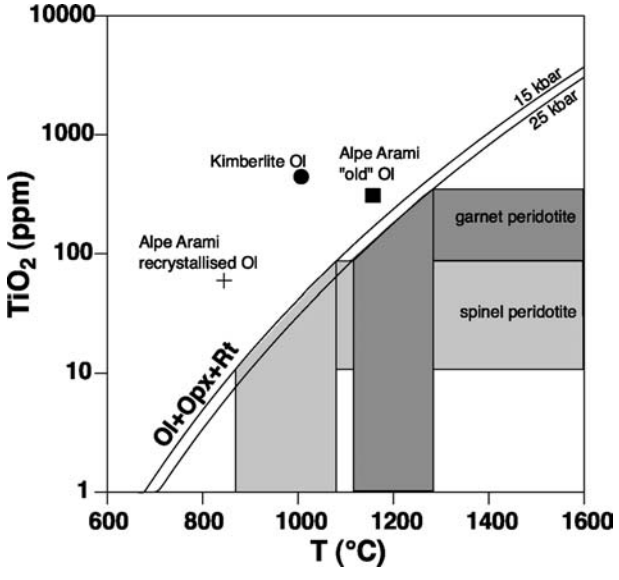

Fig. 10 Calculated TiO_2 contents of olivine buffered by Opx + Rt as a function of temperature at 15 and 25 kbar. The range of TiO_2 contents of olivine from garnet peridotites (*dark grey band*) and spinel peridotites (*light grey band*) are shown. At temperatures higher than the saturation level, no free Ti-phase is expected whereas at lower temperatures, the formation of a Ti-phase such as rutile, ilmenite or Ti-pargasite is possible. Also shown are the estimated positions of a kimberlite olivine, and of structurally old Ti-rich olivine and olivine neoblasts from Alpe Arami. The position of olivine above the anhydrous saturation indicates the presence of an additional Ti-component such as a Ti-clinohumite defect

Conclusions

1. The TiO_2 content of olivine is strongly dependent on the paragenesis. Olivine coexisting with spinel (Mg_2TiO_4) contains the highest concentration of TiO_2. Hence, the simple assumption that the maximum TiO_2 content of a mineral is reached when it is buffered with rutile is incorrect. Phase relations and mineral compositions suggest that Ti substitutes directly for Si at temperatures of 1,200–1,500°C under anhydrous conditions.
2. The solubility of TiO_2 in olivine in a buffered paragenesis strongly decreases with decreasing temperature. Olivine from garnet peridotites reach TiO_2 saturation under anhydrous conditions at 1,100–1,300° whereas olivine from spinel peridotites gener-

ally reach saturation below 1,050°C. Cooling is therefore a plausible mechanism to explain the exsolution of Ti-rich phases from olivine.

3. There is no evidence for an increase in the solubility of Ti in olivine with increasing pressure. Therefore, ilmenite rods in olivine from orogenic peridotites are not indicative of an ultra-deep origin.
4. H_2O is likely to play an important role in the incorporation of Ti in olivine and the formation of ilmenite rods. Hydration of the Mg_2TiO_4 component in olivine may produce Ti-clinohumite defects which break down to olivine + ilmenite rods + H_2O during metamorphism beyond the stability of the defects.

Acknowledgments We thank the Australian Research Council and the Swiss National Science foundation (JH) for financial support, P. Ulmer and G. Brey for reviews of the paper, W.O. Hibberson and D.R. Scott for assistance with sample preparation, S.E. Kesson for X-ray powder diffraction and Reitveld refinement, and N.G. Ware for assistance with electron microprobe analyses.

References

Boyd FR, Nixon PH (1978) Ultramafic nodules from the Kimberley pipes, South Africa. Geochim Cosmochim Acta 42:1367–1382

Bozhilov KN, Green HW, Dobrzhinetskaya L (2003) Quantitative 3D measurement of ilmenite abundance in Alpe Arami olivine by confocal microscopy: Confirmation of high-pressure origin. Am Mineral 88:596–603

Capobianco CJ, Amelin AA (1994) Metal-silicate partitioning of nickel and cobalt: The influence of temperature and oxygen fugacity. Geochim Cosmochim Acta 58:125–140

Chatterjee ND, Krüger R, Haller G, Olbricht W (1998) The Bayesian approach to an internally consistent thermodynamic database: theory, database, and generation of phase diagrams. Contrib Mineral Petrol 133:149–168

Dalton JA, Lane SJ (1996) Electron microprobe analysis of Ca in olivine close to grain bondaries: the problem of secondary X-ray fluorescence. Am Mineral 81:194–201

Dobrzhinetskaya L, Green HW, Wang S (1996) Alpe Arami: a peridotite massif from depths of more than 300 kilometers. Science 271:1841–1845

Dobrzhinetskaya L, Bozhilov KN, Green HW (1999) The solubility of TiO_2 in olivine: implications for the mantle wedge environment. Chem Geol 160:357–370

Feenstra A, Engi M (1998) An experimental study of the Fe–Mn exchange between garnet and ilmenite. Contrib Mineral Petrol 131:379–392

Green HW, Dobrzhinetskaya L, Riggs EM, Zhen-Ming J (1997) Alpe Arami: a peridotite massif from the Mantle Transition Zone? Tectonophysics 279:1–21

Gudfinnson GH, Wood BJ (1998) The effect of trace elements on the olivine—wadsleyite transformation. Am Miner 83:1037–1044

Hacker BR, Sharp T, Zhang RY, Liou JG, Hervig RL (1997) Determining the origin of ultrahigh-pressure lherzolites. Science 278:702–704

Hamilton DL, Henderson CMB (1968) The preparation of silicate compositions by a gelling method. Miner Mag 36:832–838

Hervig RL, Smith JV, Dawson JB (1986) Lherzolite xenoliths in kimberlites and basalts: petrogenetic and crystallochemic significance of some minor and trace elements in olivine, pyroxenes, garnet and spinel. Trans R Soc Edinburgh Earth Sci 77:181–201

Holland TJB, Powell R (1998) An internally consistent thermodynamic dataset for phases of petrological interest. J Metamorphic Geol 16:309–343

Jones A, Smith JV, Dawson JB (1982) Mantle metasomatism in 14 veined peridotites from Bultfontein mine, South Africa. J Geol 90:435–453

Kamb B (1968) Structural basis of the olivine-spinel stability relation. Am Miner 53:1439–1455

Köhler TP, Brey GP (1990) Calcium exchange between olivine and clinopyroxene calibrated as a geothermobarometer for natural peridotites from 2 to 60 kb with applications. Geochim Cosmochim Acta 54:2375–2388

MacGregor ID (1969) The System MgO-SiO_2-TiO_2 and its bearing on the distribution of TiO_2 in basalts. Am J Sci 267A:342–363

McDonough WF, Stosch H-G, Ware NG (1992) Distribution of titanium and the rare earth elements between peridotitic minerals. Contrib Mineral Petrol 110:321–328

Nimis P, Trommsdorff V (2001) Revised thermobarometry of Alpe Arami and other garnet peridotites from the Central Alps. J Petrol 42:103–115

O'Neill HSC (1998) Partitioning of Fe and Mn between ilmenite and olivine at 1100°C: constraints on the thermodynamic mixing properties of $(Fe,Mn)TiO_3$ ilmenite solid solutions. Contrib Mineral Petrol 133:284–296

O'Neill HSC, Scott D (2004) The free energy of formation of Mg_2TiO_4 (synthetic qandelite), an inverse spinel with configurational entropy. Eur J Min (in press)

Paquin J, Altherr R (2001) New constraints on the P-T evolution of the Alpe Arami garnet peridotite body (Central Alps, Switzerland). J Petrol 42:1119–1140

Post JE, Bish DL (1989) Rietveld refinement of crystal structures using powder X-ray diffraction data. In: Bish DL, Post JE (eds) Modern powder diffraction. Mineralogical Society of America, Washington, pp 277–308

Reusser E, Risold AC, Günther D, Trommsdorff V (1998) Bulk Ti-content of ilmenite-bearing olivine from garnet lherzolites. EOS Trans Am Geophys Union 79:F953–F954

Risold AC (2001) Formation of oxide inclusions in olivine from garnet peridotites (Central Alps). PhD Thesis, ETH Zürich, Nr. 14159: p 128

Risold AC, Trommsdorff V, Grobéty B (2001) Genesis of ilmenite rods and palisades along humite-type defects in olivine from Alpe Arami. Contrib Mineral Petrol 140:619–628

Tinker D, Lesher CE (2001) Solubility of TiO_2 in Olivine from 1 to 8 GPa. EOS Trans Am Geophys Union 82:F1393

Todd SS (1952) Low temparture heat capacities and entropies at 298.16 K of magnesium orthotitanate and magnesium dititanate. J Am Chem Soc 74:4669–4670

Trommsdorff V, Hermann J, Müntener O, Pfiffner M, Risold A-C (2000) Geodynamic cycles of subcontinental lithosphere in the Central Alps and the Arami enigma. J Geodynamics 30:70–92

Ulmer P, Risold AC, Trommsdorff V (1998) TiO_2 solubility in mantle olivine as a function of pressure, temperature, $a(SiO_2)$, and $f(H_2)$. EOS Trans Am Geophys Union 79:F164

Woermann E, Brezney B, Muan A (1969) Phase equilibria in the system MgO–iron oxide–TiO_2 in air. Am J Sci 267:463–479

Xirouchakis A, Hirschmann MM, Simpson JA (2001) The effect of titanium on the silica content and on mineral–liquid partitioning of mantle equilibrated melts. Geochim Cosmochim Acta 65:2201–2217

Xirouchakis A, Smirnov A, Woody K, Lindsley DH, Anderson DJ (2002) Thermodynamics and stability of pseudobrookite-type $MgTi_2O_5$ (karrooite). Am Miner 87:658–667

Young RA, Sakthivel A, Moss TS, Paiva-Santos CO (1995) DBWS-9411—an upgrade of the DBWS*.* programs for rietveld refinement with PC and mainframe computers. J Appl Cryst 28:366–367